UNCLASSIFIED

DIAGNOSTICS DEVELOPMENT FOR E-BEAM-EXCITED AIR CHANNELS

Final Technical Report
Covering the Period 1 June 1984 to 31 May 1985

November 12, 1985

By: D. J. Eckstrom, M. N. Spencer, and J. S. Dickinson

Sponsored by:

DEFENSE ADVANCED RESEARCH PROJECTS AGENCY
1400 Wilson Blvd.
Arlington, VA 22209

Monitored by:

OFFICE OF NAVAL RESEARCH
800 North Quincy Street
Arlington, VA 22217

ARPA Order No. 4128
Contract No. N00014-84-C-0718
Effective Date: 1 June 1984
Expiration Date: 31 May 1985
Principal Investigator: D. J. Eckstrom (415) 859-4398

SRI Project PYU 7782
MP Report No. 85-237

SRI International
333 Ravenswood Avenue
Menlo Park, California 94025-3493
(415) 326-6200
TWX: 910-373-2046
Telex: 334 486

UNCLASSIFIED

Accession Number: 3961

Publication Date: Nov 12, 1985

Title: Diagnostics Development for E-Beam-Excited Air Channels

Personal Author: Eckstrom, D.J.; Spencer, M.N.; Dickinson, J.S.

Corporate Author Or Publisher: SRI International, 333 Ravenswood Avenue, Menlo Park, CA 94025 Report Number: SRI PYU 7782; MP 85-237

Report Prepared for: Office of Naval Research, 800 North Quincy St., Arlington, VA 22217 Report Number Assigned by Contract Monitor: DEL 86-U-0001

Comments on Document: Archive, RRI, DEW

Descriptors, Keywords: Diagnostics Development E-beam Excite Air Channel Plasma Microwave PHERMEX Accelerator Medea Parameter Afterglow Conductivity Kinetics Benzene Photoionization Water Vapor

Pages: 00039

Cataloged Date: Nov 30, 1992

Contract Number: N00014-84-C-0718

Document Type: HC

Number of Copies In Library: 000001

Record ID: 25361

Source of Document: DEW

REPORT DOCUMENTATION PAGE

1a. REPORT SECURITY CLASSIFICATION Unclassified	1b. RESTRICTIVE MARKINGS
2a. SECURITY CLASSIFICATION AUTHORITY DARPA-CG-55	3. DISTRIBUTION/AVAILABILITY OF REPORT Approved for public release; distribution unlimited.
2b. DECLASSIFICATION/DOWNGRADING SCHEDULE	
4. PERFORMING ORGANIZATION REPORT NUMBER(S) MP 85-237	5. MONITORING ORGANIZATION REPORT NUMBER(S)
6a. NAME OF PERFORMING ORGANIZATION SRI International 6b. OFFICE SYMBOL (If applicable)	7a. NAME OF MONITORING ORGANIZATION Office of Naval Research
6c. ADDRESS (City, State and ZIP Code) 333 Ravenswood Ave. Menlo Park, CA 94025	7b. ADDRESS (City, State and ZIP Code) 800 N. Quincy Street Arlington, VA 22217
8a. NAME OF FUNDING/SPONSORING ORGANIZATION Defense Advanced Research Projects Agency 8b. OFFICE SYMBOL (If applicable)	9. PROCUREMENT INSTRUMENT IDENTIFICATION NUMBER Contract No. N00014-84-C-0718
8c. ADDRESS (City, State and ZIP Code) 1400 Wilson Blvd. Arlington, VA 22209	10. SOURCE OF FUNDING NOS. PROGRAM ELEMENT NO. 4128 Amendment 9 / PROJECT NO. / TASK NO. / WORK UNIT NO.
11. TITLE (Include Security Classification) DIAGNOSTICS DEVELOPMENT FOR E-BEAM-EXCITED AIR CHANNELS	
12. PERSONAL AUTHOR(S) D. J. Eckstrom, M. N. Spencer, and J. S. Dickinson	
13a. TYPE OF REPORT Final Technical 13b. TIME COVERED FROM 840601 TO 850531	14. DATE OF REPORT (Yr., Mo., Day) 1985 Nov. 12 15. PAGE COUNT 39
16. SUPPLEMENTARY NOTATION	

17. COSATI CODES			18. SUBJECT TERMS (Continue on reverse if necessary and identify by block number)
FIELD	GROUP	SUB. GR.	Electron beams, plasma, microwave diagnostics

19. ABSTRACT (Continue on reverse if necessary and identify by block number)

We have summarized and reviewed the results from three sets of afterglow conductivity measurements that were performed (1) in our laboratory using Febetron 706 excitation, (2) at Los Alamos National Laboratory using the PHERMEX accelerator, and (3) at McDonnell-Douglas Research Laboratory using the Medea accelerator. The results of these studies were presented in detail in our interim technical reports.

20. DISTRIBUTION/AVAILABILITY OF ABSTRACT UNCLASSIFIED/UNLIMITED ☐ SAME AS RPT. ☒ DTIC USERS ☐	21. ABSTRACT SECURITY CLASSIFICATION Unclassified
22a. NAME OF RESPONSIBLE INDIVIDUAL C. M. Huddleston	22b. TELEPHONE NUMBER (Include Area Code) (202) 394-1264 22c. OFFICE SYMBOL NG0921

The results of the three studies are in essential agreement and form an empirical basis for predicting the afterglow conductivity histories for electron beams that do not heat the air channel significantly. We find a strong sensitivity to the humidity of the test air, which necessitates consideration of that parameter in experiments and operational systems. The dry air results are in some disagreement with air chemistry model calculations, which prevents confident use of those models in their current form for predictions. That situation is expected to be worse for the humid air cases. Furthermore, neither experiment nor model addresses heated air channels, which are essential to operational systems. Thus, further work in this area is required.

The Medea experiments constitute the first channel-tracking studies with wide pulse spacing (200-500 μs). Our measurements of the DC conductivities at the optimum channel tracking conditions are in good agreement with the value of 2.5×10^9 sec^{-1} predicted by simple theory.

We present as an appendix a reprint of a paper resulting from our study of benzene ion fragmentation during photoionization with intense KrF laser pulses. We found that at high laser intensities the total ion yield was reduced below the values predicted by a rate equation model based on cross sections and intermediate state lifetimes determined in our previous measurements at low laser intensities; furthermore, extensive fragmentation of the ions was observed. These results have implications for laser channel tracking studies.

CONTENTS

FIGURES

TABLE

I INTRODUCTION

Objectives

The objectives of this contract were to develop and apply diagnostics techniques for the propagation of charged particle beams in the atmosphere, including particularly the response of the air channel to passage of the beam. These diagnostics techniques fall into two categories: (a) measurements based on air fluorescence spectroscopy, and (b) afterglow conductivity measurements based on microwave techniques. In addition, we performed a variety of auxiliary experiments to support the CPB program, usually in our area of expertise in chemical physics. During this contract period, for example, we studied the fragmentation of benzene during photoionization at high KrF laser intensities in support of the laser-guiding technique used in the Advanced Test Accelerator (ATA) at Lawrence Livermore National Laboratory (LLNL).

Scope of Activities

Our work during this contract period involved almost exclusively afterglow conductivity measurements performed in our own laboratory using Febetron 706 electron beam excitation [SDE85a], as well as at Los Alamos National Laboratory (LANL) using the PHERMEX accelerator [EDS85] and at McDonnell-Douglas Research Laboratory (MDRL) using the MEDEA accelerator [SDE85b]. Since these studies have been described in detail in the references just cited, this final technical report will consist of only a brief summary and comparison of the results from the three sets of experiments. We also include as an Appendix a reprint of the publication on benzene photofragmentation/photoionization resulting from our study mentioned above [RE85].

Approach

Our usual procedure is to develop a diagnostic technique in our laboratory and to check it out using our Febetron 706 as an electron beam source. This device produces a 3-ns-long pulse of 600-keV electrons with peak current of about 5 kA in a beam 2 cm in diameter. "Beam" is a misnomer, since the electron motion is generally governed by scattering so that the current density decreases rapidly with distance from the exit foil. The short pulses and decreasing current with distance are in contrast to accelerators used for propagation studies; hence, the electron beam excitation rates in Febetron studies are lower than appropriate to propagating beams. Nevertheless, these studies establish a baseline for accelerator tests, and allow a more extensive investigation of various parameters of the experiment than is usually possible at other laboratories.

After establishing a technique in our laboratory, we use it to perform measurements at other laboratories participating in the CPB program. Thus, during this program we made measurements on accelerators at LANL and MDRL as noted above.

The afterglow conductivity measurements cited above were performed primarily by using the microwave cavity perturbation technique, which we have described in previous reports [Ec83, SDE85a]. During this contract period, we also designed and constructed a 35-GHz microwave interferometer which, because of time constraints, was used extensively only in the PHERMEX tests [EDS85].

II EXPERIMENTAL TECHNIQUES

The propagation of an electromagnetic wave through a plasma is governed by a scalar dielectric constant, κ, which is related to the phase of the wave, and a scalar conductivity, σ, which is related to the attenuation of the wave. These parameters can be combined into a complex dielectric constant,

$$\bar{\kappa} = \kappa - j\sigma/\omega\varepsilon_o \quad , \tag{II.1}$$

or, alternately, into a complex conductivity,

$$\bar{\sigma} = \sigma + j\omega(\kappa - 1)\varepsilon_o$$

$$= \sigma_r + j\sigma_i \quad . \tag{II.2}$$

The propagation can also be expressed in terms of a complex refractive index,

$$\bar{\mu} = \mu - j\chi = \bar{\kappa}^{1/2} \quad . \tag{II.3}$$

In terms of the complex conductivities, the refractive indices can be written as

$$\left\{\begin{matrix}\mu \\ \chi\end{matrix}\right\} = \frac{1}{\sqrt{2}}\left\{\pm\left(1 + \frac{\sigma_i}{\varepsilon_o\omega}\right) + \left[\left(1 + \frac{\sigma_i}{\varepsilon_o\omega}\right)^2 + \left(\frac{\sigma_r}{\varepsilon_o\omega}\right)^2\right]^{1/2}\right\}^{1/2} \quad . \tag{II.4}$$

In a single-pass propagation experiment, the phase change of the probe beam, expressed as fringes per unit length, is

$$\Delta S = (\mu_o - \mu)/\lambda \qquad \text{cm}^{-1} \tag{II.5}$$

whereas the attenuation of the probe beam is

$$\alpha = \chi\omega/c \qquad \text{cm}^{-1} \quad . \tag{II.6}$$

Thus, if an interferometer experiment is performed in which the fringe shift and the attenuation are measured so as to determine μ and χ, respectively, it is then possible to determine σ_r and σ_i from equation (II.4).

An alternate approach that provides more sensitivity is the microwave cavity perturbation technique, which bears the same relationship to microwave interferometry as a Fabry-Perot interferometer does to a Mach-Zehnder interferometer in optics. That is, the cavity creates a standing-wave pattern that interacts with the plasma on a multipass rather than single-pass basis. The plasma causes changes in the resonant frequency, ω, and the quality factor, Q, of the cavity as given by the Slater perturbation formula

$$\Delta\left(\frac{1}{Q}\right) - 2j\,\frac{\Delta\omega}{\omega} = \frac{1}{\varepsilon_o \omega}\,\frac{\int_v \vec{J} \cdot \vec{E}\, dv}{\int_v \vec{E} \cdot \vec{E}_o\, dv} \quad . \tag{II.7}$$

When the perturbation is small enough that the electric fields retain their initial values, $\vec{E} = \vec{E}_o$, the perturbation formula can be written

$$\Delta\left(\frac{1}{Q}\right) - 2j\,\frac{\Delta\omega}{\omega} = \frac{1}{\varepsilon_o \omega}\,\frac{\int_v \bar{\sigma}(r)\, E^2(r)\, dv}{\int_v E^2(r)\, dv}$$

$$\approx \frac{\bar{\sigma}}{\varepsilon_o \omega}\,\frac{\int_{\text{plasma}} E^2(r)\, dv}{\int_{\text{cavity}} E^2(r)\, dv}$$

Again, measurements of ΔQ and $\Delta\omega$, which correspond to an attenuation and a phase shift, allow determination of the real and imaginary conductivities, respectively.

The above equations outline the relationships between measured parameters (ΔQ and $\Delta\omega$ for the cavity, α and ΔS for the interferometer) and the real and imaginary conductivities. The details of the measurements and the data analyses are given in our interim technical reports referenced above. Now, the complex conductivity terms are not directly useful (although the real conductivity is approximately equal to the desired DC-limit conductivity in many cases), but they can be used to derive several plasma parameters of immediate interest.

We note first that a plasma conductivity has two components -- first, from electrons interacting with positive ions, and second, from negative ions interacting with positive ions. Because the negative ions move so much more slowly than electrons, and because the resonant frequency (plasma frequency) of negative/positive ions is so much lower than for electrons and positive ions, the contribution from negative ions is usually neglected. However, if the ratio of number density of negative ions to number density of electrons exceeds the mass ratio of negative ions to electrons (which is of order 10^5), the contribution from negative ions will dominate the conductivities. This can happen in the late afterglow of a plasma when the electron attachment rate exceeds the electron/ion recombination rate, and almost all the free electrons are converted to negative ions. We believe this is the case in many of our measurements.

The equations that follow will be written for electrons, but they are equally valid for negative ions if the appropriate mass, velocity, collision frequency, etc., are used. Now, the complex conductivity can be written in terms of the electron mass, m_e; number density, n_e; velocity distribution function, $f(v)$; and momentum transfer collision frequency, $\nu(v)$, as

$$\bar{\sigma} = -\frac{4\pi}{3}\frac{n_e e^2}{m_e}\int \frac{1}{\nu + j\omega}\frac{df(v)}{dv}\, v^3\, dv \qquad \text{(II.8)}$$

If f and $\nu(v)$ is known (for example, if it can be assumed to be Maxwellian at an electron temperature T_e), this equation can be used to calculate the conductivities. We are more concerned with inverting the equation, that is, with determining n_e and f from the measured σ's. Again, if it is assumed that f is Maxwellian, the right-hand side of equation (II.8) can be calculated as a function of T_e for both the real and imaginary terms. The ratio of these terms can then be formed and compared with the experimental ratios of σ_r/σ_i. A unique agreement between calculated and measured ratios validates the assumptions and identifies an electron temperature. This temperature (and corresponding f) can then be used to determine n_e from equation (II.8) and the measured σ_r or σ_i. Finally, the real conductivity in the DC limit, σ_{DC}, can be evaluated from equation (II.8) by letting $\omega \ll \nu$, which leads to

$$\sigma_{DC} = -\frac{4\pi}{3}\frac{n_e e^2}{m_e}\int \frac{1}{\nu}\frac{df(v)}{dv} v^3\, dv \qquad (II.9)$$

σ_{DC} is the parameter of direct interest in analyzing the propagation of charged particle beams.

We used this rather laborious procedure to analyze the results from our Febetron experiments as reported in [SDE85a]. We also compared the plasma properties calculated that way with values calculated using the much simpler constant collision frequency approximation. As the name suggests, this approximation consists of setting $\nu(v)$ = constant in equation (II.8). This leads to the relations

$$\bar{\sigma} = \varepsilon_o \omega_p^2 \frac{\nu - j\omega}{\omega^2 + \nu^2} . \qquad (II.10)$$

where the plasma frequency, ω_p, is given by

$$\omega_p^2 = n_e e^2/m_e \varepsilon_o . \qquad (II.11)$$

With this approximation, the collision frequency can be determined simply from the ratio of real to imaginary conductivity:

$$\sigma_r/\sigma_i = - \nu/\omega \qquad \text{(II.12)}$$

and the plasma frequency can then be calculated by using this value of ν together with either the measured real or imaginary conductivity in equation (II.10).

It should be emphasized that the experimental real and imaginary conductivities are valid independent of the analysis techniques just described, and independent of whether the conductivity is due to electrons or negative ions. The accuracy of the calculated values of collision frequencies and plasma frequencies and, to a lesser extent, the DC-limit conductivities, varies with the data analysis technique and the parameter regime (e.g., low versus high pressure). Note that the exact procedure breaks down when the collision frequency falls outside the range expected for electrons (e.g., when negative ions make the dominant contribution), but that the constant collision frequency approximation still yields valid collision frequencies and plasma frequencies.

As indicated above, we analyzed the results of our Febetron experiments reported in [SDE85a] using both the exact procedure and the constant collision frequency approximation. The electron densities calculated using the approximation were in good agreement with the values from the exact calculation at low pressures, and progressively deviated to 30% smaller values at 100 torr. Because of its simplicity, versatility, and generally acceptable accuracy, we used the constant collision frequency approximation in subsequent data analyses.

III RESULTS

Electron Beam Parameters

As noted in the Introduction, we performed afterglow conductivity measurements on the Febetron electron-beam source at SRI, the PHERMEX accelerator at LANL, and the Medea accelerator at MDRL. The parameters of these devices are summarized in Table 1. The PHERMEX accelerator produced a sequence of 10 pulses spaced 20 ns apart; our results are for the afterglow following that entire pulse train. The Medea accelerator can produce two pulses spaced 200 μs or more apart. Most of our results are for single-pulse operation, but we did one measurement at 50 torr air pressure with two pulses spaced 250 μs apart.

Summary of Real Conductivity Histories

Our measurements yield directly the real and imaginary conductivities, and since the real conductivities are usually not too different from the DC-limit conductivities that are of interest in propagation studies, we emphasize those results.

Figures 1 through 6 present summaries of the σ_r (or, alternately, $\sigma_{\mu w}$) versus time histories at each pressure tested for the experiments at the three facilities (the latter nomenclature emphasizes that these values are for the microwave frequency of these experiments, rather than the DC limit). The first three figures are for synthetic air (79% N_2, 21% O_2), whereas the last three are for laboratory air, which contains varying amounts of water vapor. These figures display the general features of afterglow plasmas. That is, the conductivities decay approximately exponentially, with the time constant for decay increasing with decreasing pressure down to about 10 torr and then decreasing again with further decreases in pressure; the decay times are also considerably shorter for laboratory air than for synthetic air.

In results from the three facilities are in reasonably good agreement, as can be seen if the figures are overlaid. Careful comparison shows that the

Table 1

COMPARISON OF ELECTRON BEAM SOURCES

	Pulse Width	Voltage	Current
Febetron (SRI International)	3 ns	600 keV	5000 A
Medea (McDonnell-Douglas)	8 ns	1 MeV	6500 A
Phermex (Los Alamos National Lab) (10 pulses/20 ns apart)	3 ns	25 MeV	330 A

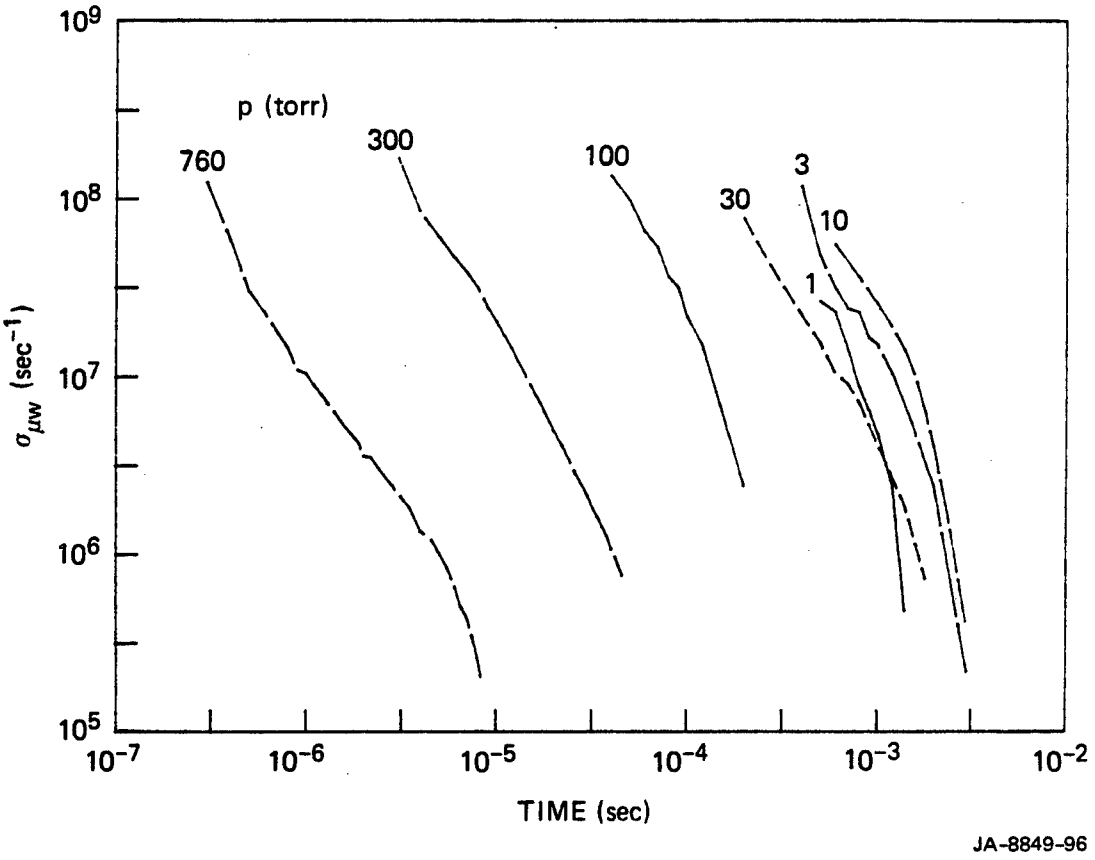

FIGURE 1 REAL CONDUCTIVITY HISTORIES FOR SYNTHETIC AIR EXCITED BY THE FEBETRON ELECTRON BEAM

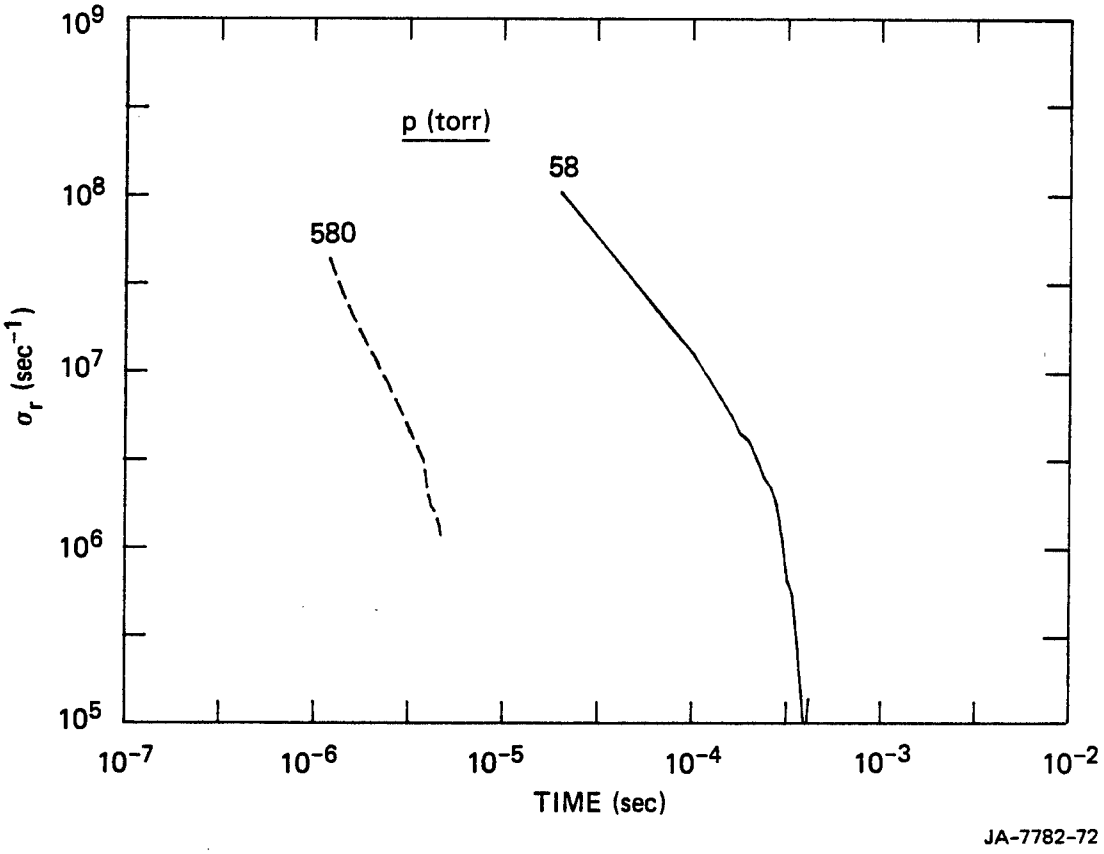

FIGURE 2 REAL CONDUCTIVITY HISTORIES FOR SYNTHETIC AIR EXCITED BY THE PHERMEX ELECTRON BEAM

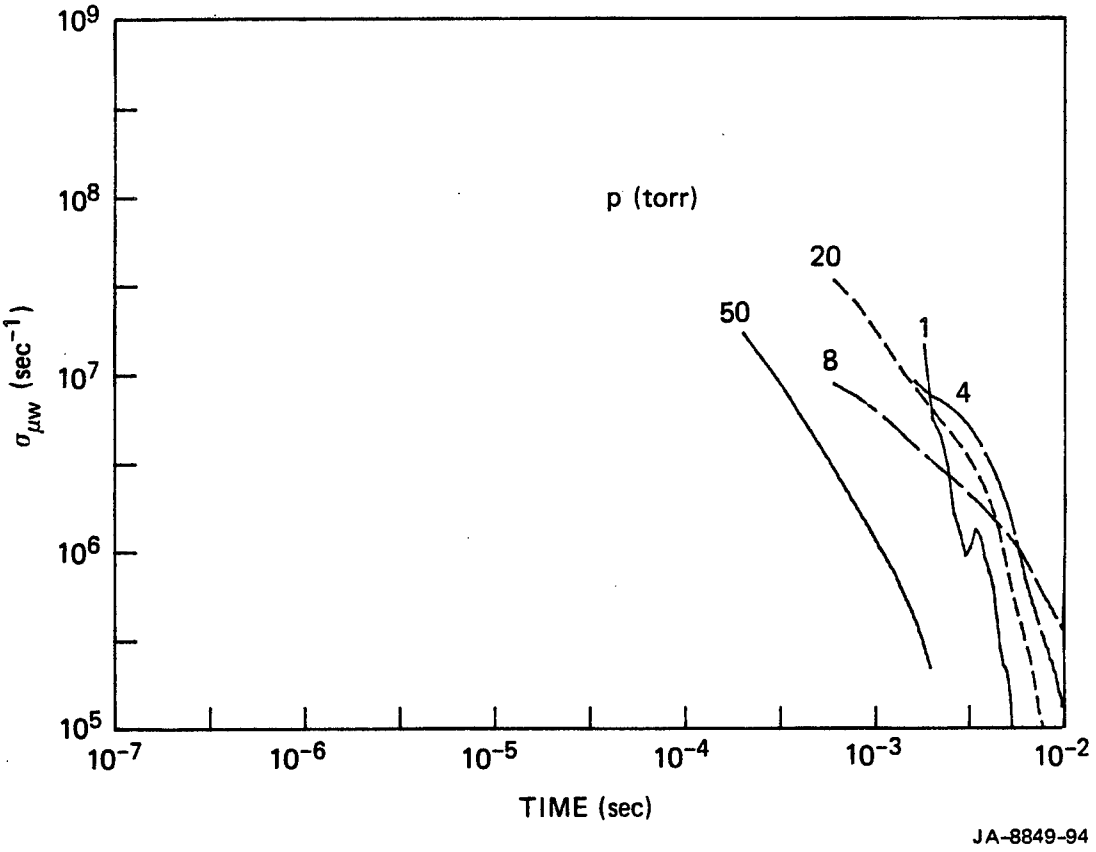

FIGURE 3 REAL CONDUCTIVITY HISTORIES FOR SYNTHETIC AIR EXCITED BY THE MEDEA ELECTRON BEAM

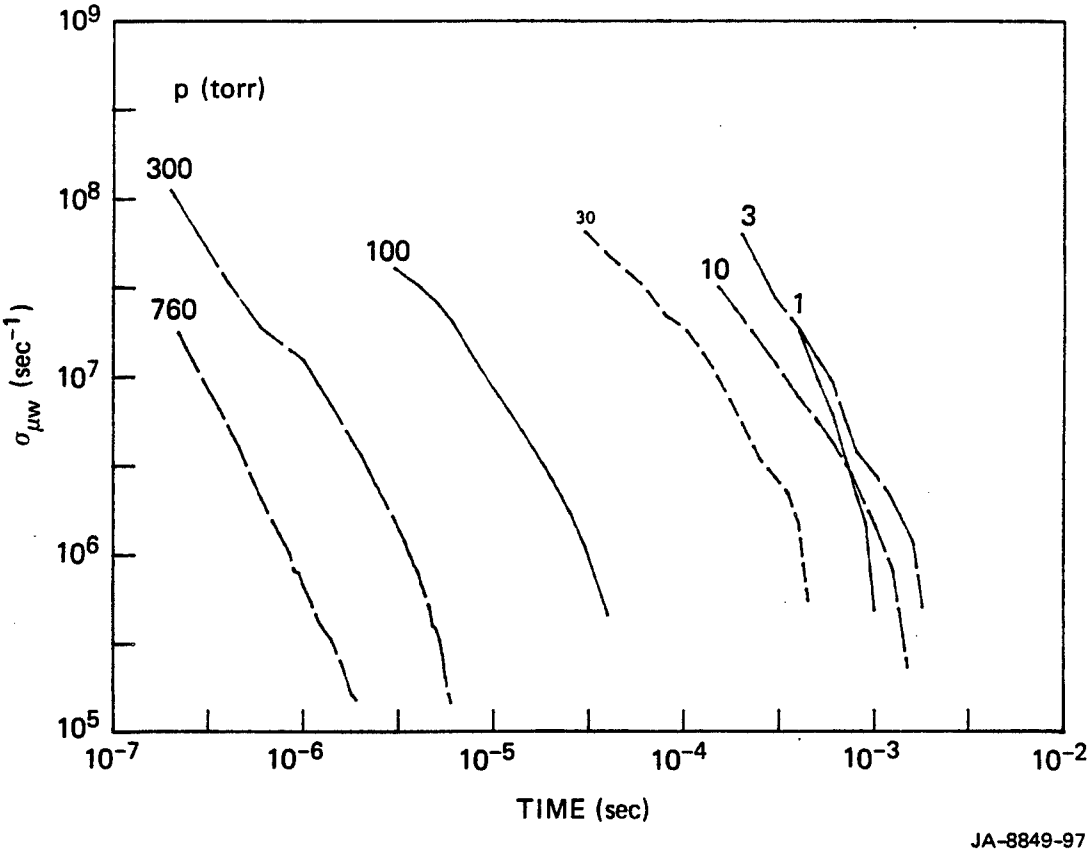

FIGURE 4 REAL CONDUCTIVITY HISTORIES FOR LABORATORY AIR EXCITED BY THE FEBETRON ELECTRON BEAM

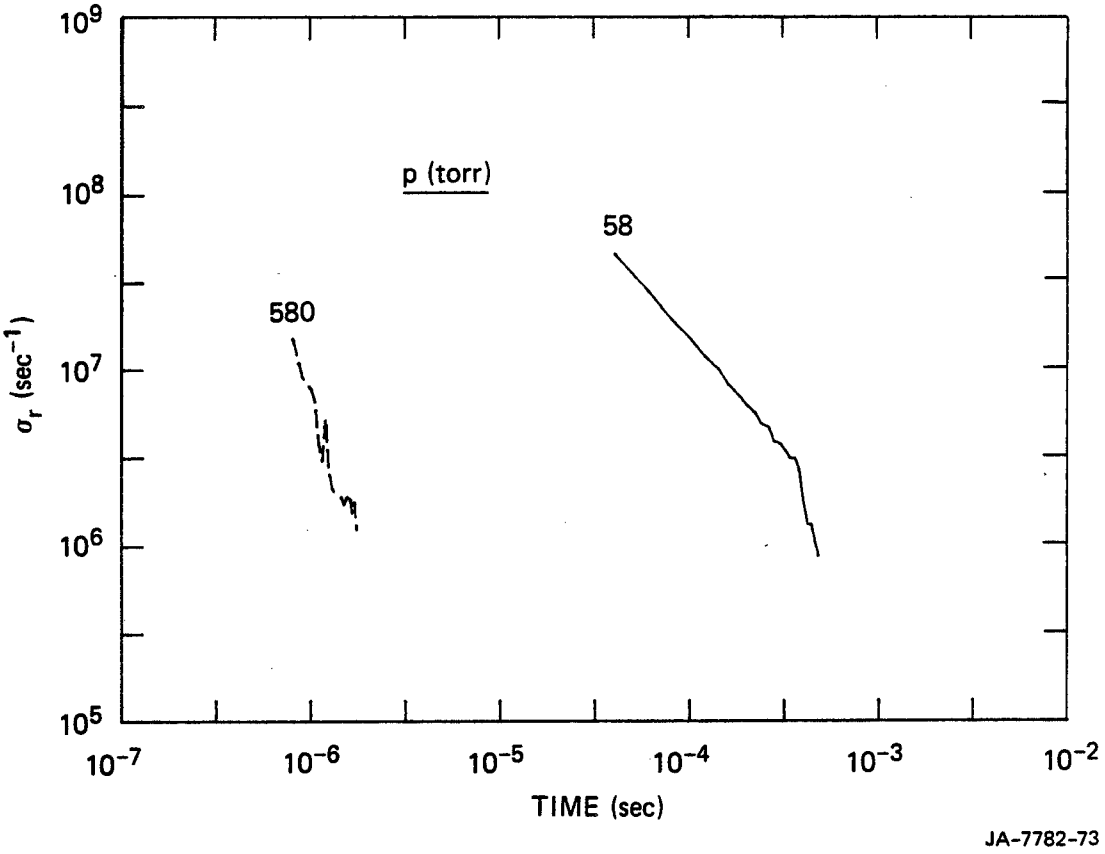

FIGURE 5 REAL CONDUCTIVITY HISTORIES FOR LABORATORY AIR EXCITED BY THE PHERMEX ELECTRON BEAM

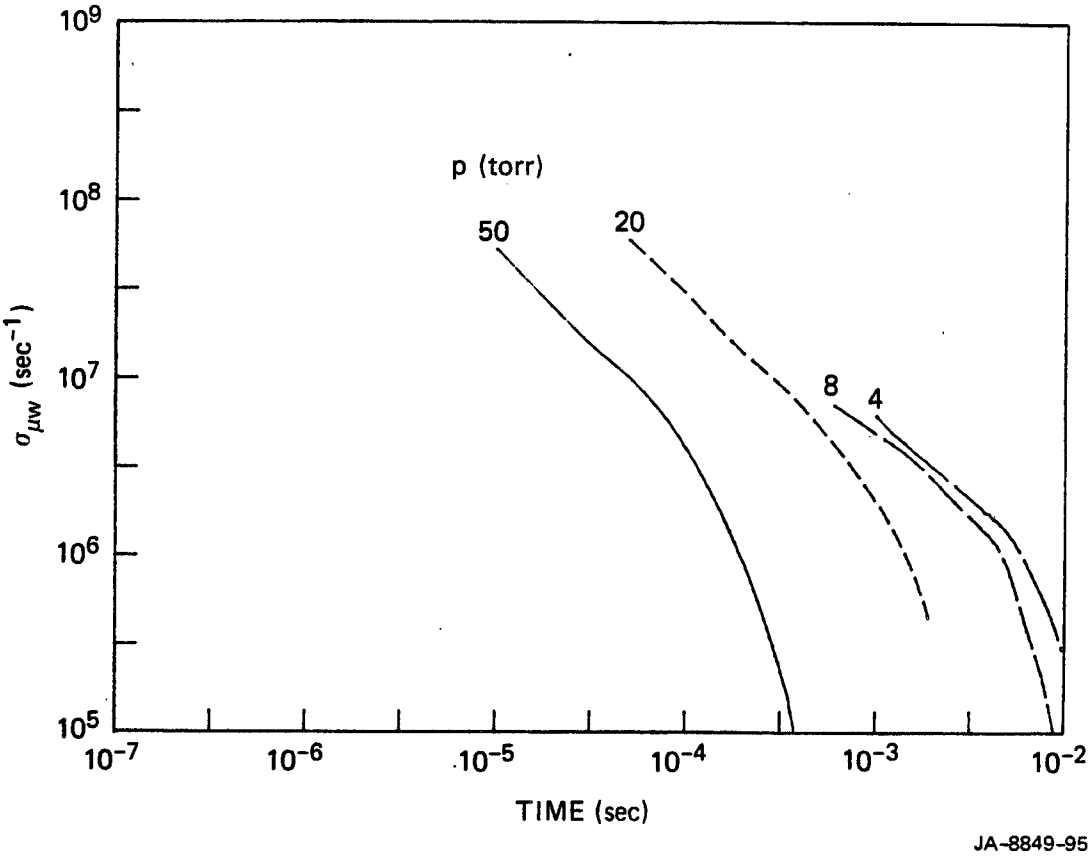

FIGURE 6 REAL CONDUCTIVITY HISTORIES FOR LABORATORY AIR EXCITED BY THE MEDEA ELECTRON BEAM

decays for $p \leq 10$ torr are longer in the Medea experiments than in the Febetron experiments. We have shown [SDE85a] that these low pressure decays are governed by diffusion, and the presence of a quartz liner in the experiments on the Febetron but not on Medea makes diffusion distances (and therefore times) shorter in the former experiments. The differences between laboratory air and synthetic air (and also some of the minor discrepancies between results from the different facilities) are due to water vapor, as we will demonstrate below.

Effects of Water Vapor

Figures 1 through 6 show that conductivity decays in humid air are much faster than in dry air. We quantified this effect in a series of experiments at 30 torr using Febetron excitation [SDE85a]. We began by drying synthetic air as well as possible (p_{water} = 0.012 torr), and then systematically increasing the humidity in steps up to p_{water} = 3.3 torr. The results are shown in Figure 7, where we see a factor of 30 decrease in the decay time from the driest to wettest case. Synthetic air as it came from the cylinder contained approximately 0.04 torr. This extreme sensitivity to moisture content causes considerable scatter in measurements of afterglow conductivity decays, but more important, it may cause day-to-day or site-to-site variations in the time for the afterglow conductivity to decay to optimum channel-tracking conditions in CPB applications involving repetitively pulsed accelerators.

Electron Density Histories

We pointed out above that the conductivities measured in these experiments contain contributions from both electrons and negative ions. We generally cannot distinguish between the two sources, and our only evidence for the importance of the ionic contribution is when the calculated momentum-transfer collision frequency, ν, is inconsistent with the values that have been measured for electrons colliding with the molecular constituents of air. We do find that to be the situation for many tests, usually involving laboratory air at higher pressures, and these cases have been documented in our interim technical reports.

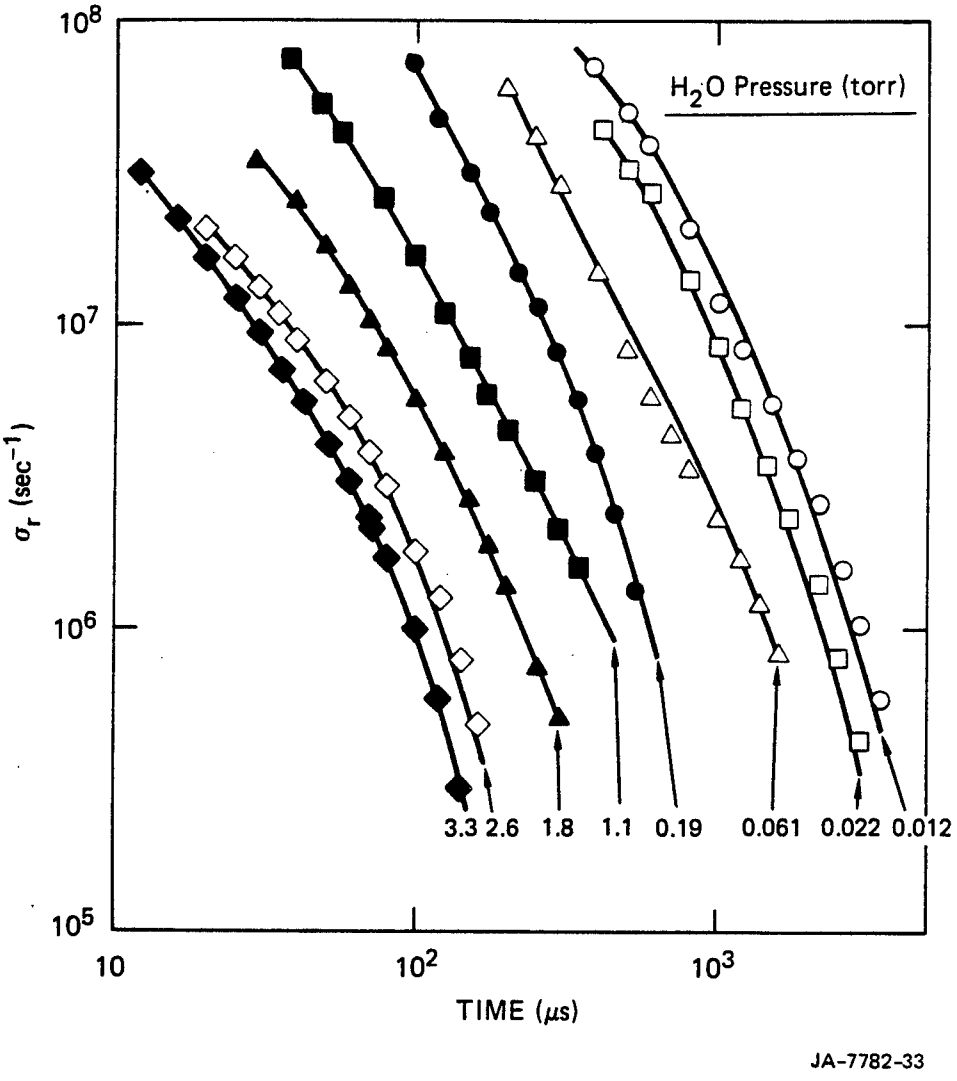

FIGURE 7 REAL CONDUCTIVITY HISTORIES FOR 30 TORR OF SYNTHETIC AIR WITH VARYING AMOUNTS OF WATER VAPOR

The plasma frequency determined experimentally can also be a sum of contributions from electrons and negative ions. However, as a simple means of comparing various results, we have treated the plasma frequency as due only to electrons and have calculated electron density histories using equation (II.11). These values are presented for each set of experiments in the relevant report. In many cases, the histories exhibit an exponential decay, and we have calculated a decay constant in each case. The decay rates are presented in Figure 8 for all the air data. Since we expect the dominant conductivity decay mechanism in the late afterglow to be electron attachment to oxygen, we have also plotted the rate for this three-body process with dry "air" as the third body.

The decay rates for pressures above 30 torr vary with the same p^2 dependence as expected for the electron attachment process, but the absolute magnitudes are 6 to 100 times smaller, depending on the experiment. As expected from the conductivity histories, the rates for dry air are smaller than for laboratory air. Also, the rates from the Medea experiments are slower than those from the Febetron tests.

Below 10 torr, ambipolar diffusion becomes a dominant plasma loss process, and the decay rates approach a p^{-1} dependence. We commented above on geometric differences between the Febetron and Medea experiments that account for their different diffusional loss rates.

Double-Pulse Effects

We have made only one measurement of conductivity decays from widely spaced pulses to date,— that on the Medea accelerator at 50-torr laboratory air [SDE85b]. The results are shown in Figure 9. A careful comparison of the decays from the two pulses shows that the decay is slightly longer following the second pulse than following the first pulse. Most of the difference can be attributed to the fact that the first pulse creates a density channel, and the reduced collision rate in that channel slows down the kinetic processes. In addition, the elevated temperature in the channel changes the free electron/attached electron equilibrium in favor of free electrons, which raises the conductivity and slows the decay. These effects will become very important for more intense beams and a greater number of sequential pulses.

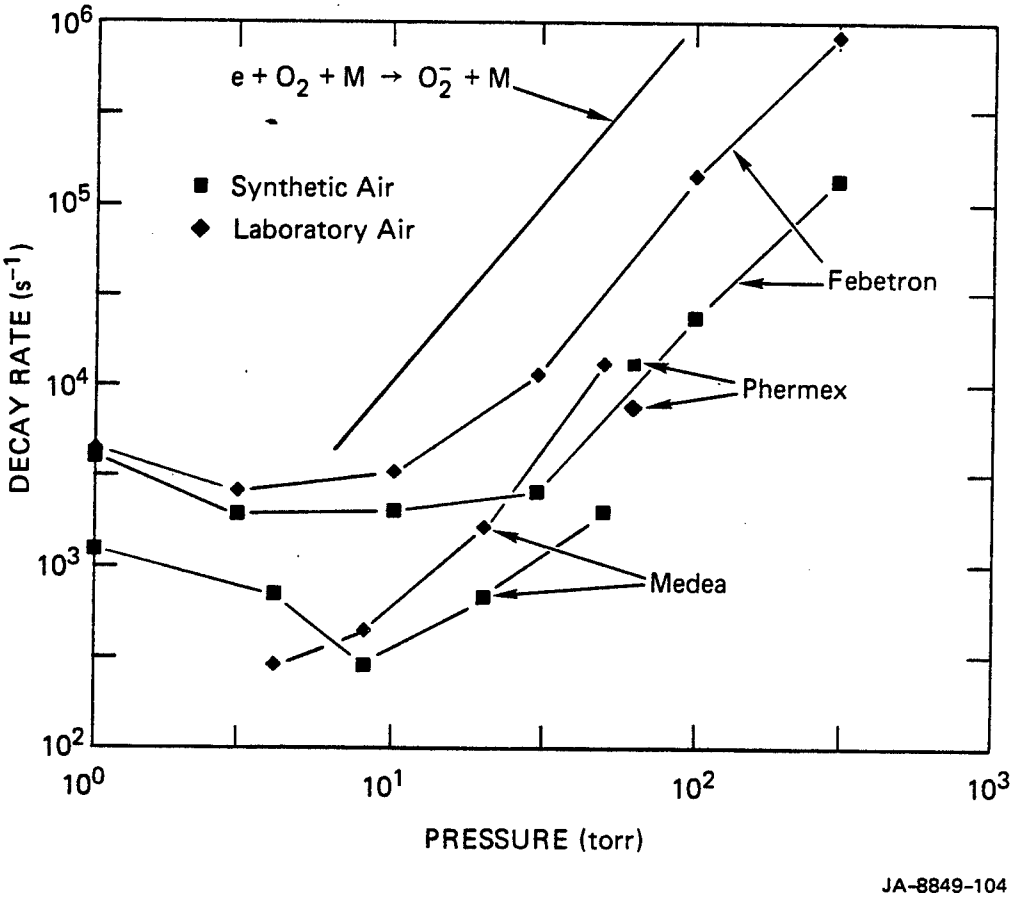

FIGURE 8 ELECTRON DENSITY DECAY RATES IN E-BEAM-EXCITED AIR

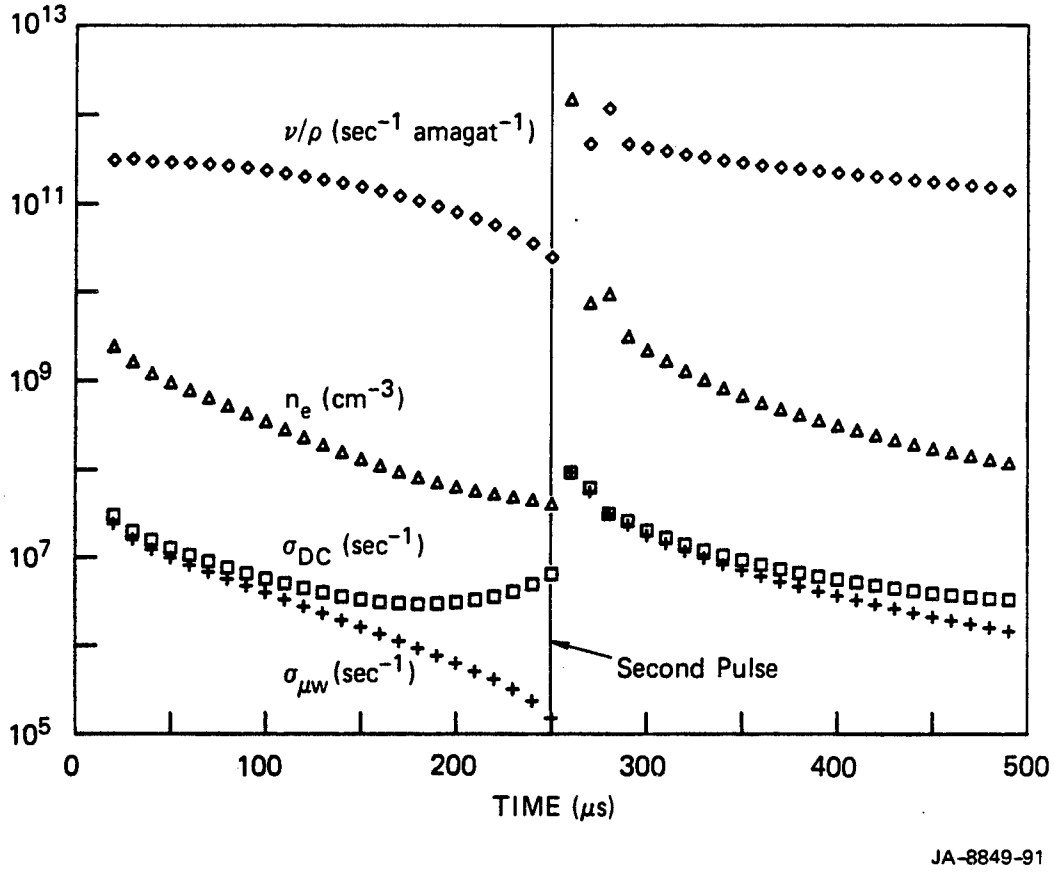

FIGURE 9 DOUBLE-PULSE AFTERGLOW CONDUCTIVITY DECAY HISTORIES FOR 50-Torr LABORATORY AIR

IV DISCUSSION

Status of Afterglow Conductivity Measurements

The general good agreement between the three sets of experiments on accelerators with different characteristics indicates that the characteristics of conductivity decay as a function of pressure are known for cold channels. We emphasize that these are cold channels, since the highest temperature we can document is approximately 450 K in the case of the Medea experiments [SDE85b]. We also emphasize that the conductivity histories are known only empirically; attempts to model the conductivity histories using air chemistry codes are limited to a preliminary effort by Ali [Al83].

Our results to date have established an extreme sensitivity of the conductivity decay rate to water vapor content of the air. Furthermore, the decay rates for dry air do not follow simple air chemistry models, and even the complex air chemistry code of Ali did not satisfactorily predict the dry air results [EDS84]. At this time, the prospect of predicting the humid air results seems quite remote, and we have little indication what effect channel heating will have on the conductivity decays. This uncertainty emphasizes the importance of continuing our measurements on higher intensity beams like the Advanced Test Accelerator at Lawrence Livermore National Laboratory in order to establish an optimum pulse interval for channel tracking in realistic charged particle beam systems.

Implications for Channel Tracking

Simple theory [HL84] indicates that the optimum DC conductivity for channel tracking is approximately

$$4\pi \sigma_{DC} a/c = 0.1 \qquad (4.1)$$

where a is the beam radius and c is the speed of light. For beam radii from 0.2 to 1 cm, this gives $\sigma_{DC} = (0.2 - 1.2) \times 10^9$ sec^{-1}.

The only tracking experiments to date were performed on the Medea accelerator at MDRL [LR85]. Those measurements were made over a range of pressures from 1 to 50 torr, and optimum tracking occurred at 4 and 8 torr when the interpulse spacing was 200 to 500 μs. Our conductivity measurements indicated that σ_{DC} was indeed near the expected value of 2.5×10^8 sec^{-1} for those pressures and afterglow times [SDE85b].

If the decay rates observed to date for cold beams are indicative of the response to more intense beams, the implication for repetitively pulsed accelerators is rather severe. That is, from Figures 1 or 4, we see that at 760 torr the conductivity passes through the 10^9 sec^{-1} range in $\ll 1$ μs. Pulsing an accelerator that quickly will surely present a technological challenge. It would seem that the conductivity decay rate in a hot channel will have to be very much reduced compared to a cold channel to make channel tracking a viable concept.

Kinetics Puzzles

We pointed out in discussing Figure 8 that the electron-density decay rates (really, the plasma frequency decay rates) are much longer than the electron attachment decay rates, even though electron attachment should be the dominant decay mechanism in the late afterglow. The differences are more pronounced for dry air than for wet air, and the differences increase with increasing energy deposition rate in the channel. Similar effects were observed in afterglow conductivity decays from microwave breakdown experiments in air [SML60].

If the conductivity is in fact due to electrons, this discrepancy must be due to a combination of a reduction of the attachment rate in the channel environment and a countervailing detachment process that maintains the free electron density. In the first case, the results of [MCA72] show that with an air mixture of N_2 and O_2 as the stabilizing third body, the electron attachment rate to O_2 increases with electron temperature to 0.07 eV and then decreases, so that the value at 1 eV is about 1/10th of the room temperature value. Since the electron temperatures deduced in our experiments are less than 0.2 eV for pressures of 10 torr and above [SDE85a], this effect should

cause no more than a factor of two reduction of the attachment rate. In the second case, there has been speculation for a long time [e.g., CPB62] that electron attachment in afterglows could be balanced by collisional detachment by vibrationally excited molecules or by metastable electronically excited molecules [e.g., $O_2(^1\Delta)$]. Since the concentrations of such excited molecules increases with electron-beam excitation rate, the collisional detachment mechanism would make decays slower when the energy deposition rate was higher, in accord with our experimental observations.

An alternate possibility is that the conductivities we measure are due to negative ions rather than to electrons, which we have inferred to be the case in some of our experiments. Then the decay should be due to an ion/ion recombination process rather than electron attachment. There are two problems with this explanation. First, the recombination can be either of the dissociative type, which is independent of neutral gas pressure, or of the three-body type, which is first order in gas pressure. Neither type should create the apparent p^2 dependence of the decay rate exhibited by the results of Figure 8. Second, a recombination process leads to a charge density decay rate that has the form $n^{-1} \propto t$. This dependence can be difficult to distinguish from an exponential decay when the variation is only over a small range, but most of our data spans at least two orders of magnitude and in most cases the decays are much closer to exponential than to recombination in shape.

It will require an extensive air chemistry modeling study to resolve these kinetic issues and to form a basis for extrapolation to other channel conditions. The results presented in our three interim reports form a sound benchmark for evaluation of the modeling study.

V CONCLUSIONS

We have summarized and reviewed the results from three sets of afterglow conductivity measurements that were performed (1) in our laboratory using Febetron 706 excitation, (2) at Los Alamos National Laboratory using the PHERMEX accelerator, and (3) at McDonnell-Douglas Research Laboratory using the Medea accelerator. The results of these studies were presented in detail in our interim technical reports.

The results of the three studies are in essential agreement and form an empirical basis for predicting the afterglow conductivity histories for electron beams that do not heat the air channel significantly. We find a strong sensitivity to the humidity of the test air, which necessitates consideration of that parameter in experiments and operational systems. The dry air results are in some disagreement with air chemistry model calculations, which prevents confident use of those models in their current form for predictions. That situation is expected to be worse for the humid air cases. Furthermore, neither experiment nor model addresses heated air channels, which are essential to operational systems. Thus, further work in this area is required.

The Medea experiments constitute the first channel-tracking studies with wide pulse spacing (200-500 μs). Our measurements of the DC conductivities at the optimum channel tracking conditions are in good agreement with the value of 2.5×10^9 sec^{-1} predicted by simple theory.

We present as an appendix a reprint of a paper resulting from our study of benzene ion fragmentation during photoionization with intense KrF laser pulses. We found that at high laser intensities the total ion yield was reduced below the values predicted by a rate equation model based on cross sections and intermediate state lifetimes determined in our previous measurements at low laser intensities; furthermore, extensive fragmentation of the ions was observed. These results have implications for laser channel tracking studies.

REFERENCES

CPB62 L. M. Chanin, A. V. Phelps, and M. A. Biondi, Phys. Rev. 128,219 (1962).

Ec83 D. J. Eckstrom, "Diagnostics Development for E-Beam Excited AirChannels. Conductivity Measurements in Air Afterglows,"Semiannual Technical Report No. 2, Contract N00014-81-C-0208,SRI International (March 1983).

EDS84 D. J. Eckstrom, J. S. Dickinson, and M. N. Spencer, "Diagnostics Development for E-Beam-Excited Air Channels," Final Technical Report, Contract N00014-81-C-0208, SRI International (November1984).

EDS85 D. J. Eckstrom, J. S. Dickinson, and M. N. Spencer, "Diagnostics Development for E-Beam Excited Air Channels. Conductivity Measurements on the PHERMEX Electron Beam," Technical Report No. 2, Contract N00014-84-C-0718, SRI International (July 1985).

HL84 B. Hui and M. Lampe, Naval Research Laboratory (quoted by J. C. Leader, McDonnell-Douglas Research Laboratory, private communication).

LR85 J. C. Leader and E. A. Rose, McDonnell-Douglas Research Laboratory (private communication).

MCA72 D. L. McCorkle, L. G. Christophorou, and V. E. Anderson, J. Phys. B: Atom. Molec. Phys. 5, 1211 (1972).

RE85 M. Rossi and D. J. Eckstrom, Chem. Phys. Lett. 120, 118 (1985).

SDE85a M. N. Spencer, J. S. Dickinson, and D. J. Eckstrom, "Diagnostics Development for E-Beam Excited Air Channels. Afterglow Conductivity Studies of the Febetron Electron Beam," Technical Report No. 1, Contract N00014-84-C00718, SRI International (July 1985).

SDE85b M. N. Spencer, J. S. Dickinson, and D. J. Eckstrom, "Diagnostics Development for E-Beam Excited Air Channels. Conductivity Measurements on the Medea Electron Beam," Technical Report No. 3, Contract N00014-84-C-0718, SRI International (September 1985).

SML60 M. C. Sexton, M. J. Mulcahy, and J. J. Lennon, in Proc. Fourth Int'l. Conf. on Ionization Phenomena in Gases," ed. N. R. Nilsson, North-Holland Publishing Co., Amsterdam (1960).

APPENDIX

Quantitative Aspects of Benzene Photoionization
At 248 nm

by

M. Rossi and D. J. Eckstrom

Reprinted From:

Chemical Physics Letters, Volume 120, Number 2

4 October 1985

QUANTITATIVE ASPECTS OF BENZENE PHOTOIONIZATION AT 248 nm

Michel ROSSI and D.J. ECKSTROM

Chemical Physics Laboratory, SRI International, Menlo Park, CA 94025, USA

Received 10 June 1985; in final form 28 July 1985

We have carefully remeasured the mass distribution of ions resulting from photoionization of benzene at 248 nm. The fragmentation occurs at lower intensities than previously indicated, beginning below 2 MW/cm^2. At 17 MW/cm^2, the parent ion constitutes only 12.5% of the total, while at 110 MW/cm^2, C^+ constitutes 24% of the yield. The functional dependence of the absolute photoionization yield as a function of laser power cannot be described by a simple four-level kinetic model successfully used to describe the absolute MPI yield at low power. Instead, a highly excited neutral intermediate is postulated that can either autoionize or photodissociate upon absorption of an additional photon.

1. Introduction

It is well known that organic molecules produce fragment ions as well as the parent ions when they are multiphoton ionized at high laser intensities [1–5]. However, there is some question about the quantitative accuracy of previous studies carried out using excimer lasers because of the difficulty of accurately specifying the laser intensity in the focal volume of these multimode lasers. Furthermore, there are no quantitative data on absolute ion yields upon resonant two-photon ionization at 248 nm at higher intensities. Such data are urgently needed in order to test or expand models for resonant MPI in polyatomic molecules. Because of the importance of the results to studies of the guiding of electron beams by preionized channels [6], we have repeated the measurements for benzene photoionized by a KrF laser, taking particular care in the determination of the focused laser intensity. In this paper we report on fragmentation patterns of benzene as a function of laser power at 248 nm and on absolute yields for resonant MPI of benzene at high laser power using the low-power results of Bischel et al. [7] as calibration points.

2. Experimental

We used a Lambda-Physik model EMG 101 excimer laser operated with standard stable resonator optics so that it produced 180 mJ pulses of 14 ns full width at half maximum in a beam 0.7 × 2.2 cm^2. An aperture of 0.35 cm diameter isolated the uniform center of the beam. This aperture was focused with a 5 cm focal length lens unto a second "pinhole" aperture. The calculated focal diameter at the pinhole was 1.13 × 10^{-4} cm. However, transmission measurements through pinholes of different diameters showed that the focal diameter was, in fact, only marginally smaller than the 0.025 cm diameter pinhole used in all subsequent experiments to define the focal diameter of the laser beam.

The power dependence of the resonant two-photon ionization of benzene was studied by monitoring the ion signal as a function of the distance between aperture II and focusing lens L1 (fig. 1) with aperture II being stationary. For all but the highest power (2.7 × 10^8 W/cm^2), the focused laser beam was vignetted by aperture II so that its homogeneous illumination was achieved throughout the study. We estimate that the maximum power transmitted through the pinhole was larger than the nominal value quoted by about 10–20% due to the fact that the focal diameter was slightly smaller than the 0.025 mm diameter pinhole

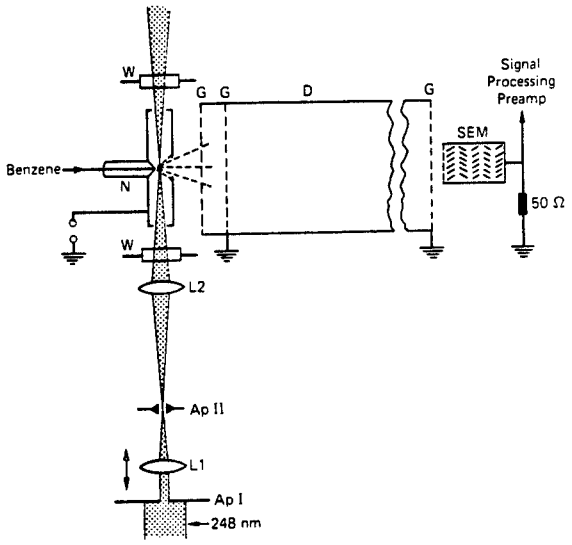

Fig. 1. Schematic of experimental apparatus for the measurement of the MPI fragmentation of benzene at 248 nm. Ap I, II, apertures; L1, L2, lenses; W, quartz window; N, tungsten needle with 40 μm diameter capillary; G, grounded grid; D, field free drift section; SEM, secondary electron multiplier.

(aperture II, fig. 1). This systematic error, however, applies only to the highest power data taken in each run, because vignetting of the beam was achieved for all other (lower) laser powers.

The pinhole aperture was imaged with unit magnification into the center of the ionization region using a 30 cm focal length lens. We measured the laser energy with a Scientech energy meter after the imaging lens but before the cell window. The maximum intensity in the focal volume based on the diameter of the pinhole, the measured laser energy, and the measured fwhm of the laser pulse, was 110 MW/cm^2. We reduced the intensity to values as low as 4.0 MW/cm^2 by moving the first lens away from the pinhole so that the laser beam passed through a focus and was diverging at the pinhole. We also made measurements at 2.3 MW/cm^2 using the apertured beam from the laser with no focusing.

Benzene was introduced into the ionization region through a tungsten capillary nozzle of 40 μm diameter, which was connected to a reservoir containing benzene at lower than ambient temperature, thus maintaining a constant pressure. The ionization chamber was maintained at a pressure of about 10^{-6} Torr, so we assume the benzene formed an effusive collisionless free jet that diverged gradually away from the orifice. The image of the pinhole was adjusted to produce the maximum ion signal for each laser intensity, which presumably occurs when the focus is just at the exit of the orifice. Note that the laser Rayleigh range was much greater than the orifice diameter, so that the intensity should have been uniform across the width of the jet.

As will be discussed later, our irradiation conditions do not lead to either saturation or photobleaching of the irradiated volume, even at the highest laser powers achieved. In view of the fact that we only ionize 10% of the sample at the highest laser powers, we took particular care to align the focal region of the beam with the jet to achieve maximum overlap. This was done by reflecting the laser beam before it entered the TOF mass spectrometer through window W (fig. 1) and searching for the position of the image of aperture II. The position of this image was brought to overlap with the jet by adjusting the position of aperture II and focal lens L2. Final "fine tuning" was achieved by maximizing the total ion signal through laser beam steering.

The ions produced were measured using a time-of-flight mass spectrometer [8] with a 2.9 kV accelerating voltage and a secondary electron multiplier detector. The voltage applied to the SEM was 2.6 kV in most experiments, but was reduced to 2.1 kV for experiments at the highest laser intensities in order to avoid saturation effects. In addition, it was necessary to decrease the stagnation presssure behind the nozzle for experiments at higher laser powers because of space charge effects on the ion flight time. We changed the benzene pressure from 0.8 to 80 Torr by cooling the benzene reservoir from room temperature to −30°C. We assume that all ions were detected with equal sensitivity, regardless of mass. When the focal region was moved vertically so that the laser beam missed the jet, the ion signal decreased essentially to zero, indicating the absence of background ionization.

The entire apparatus is shown schematically in fig. 1.

3. Results and discussion

The distribution of ion masses measured at each

Table 1
Percentage ion mass distribution resulting from 248 nm photoionization of benzene at selected laser intensities (W/cm^2)

Species	Mass	2.3(6)	3.95(6)	7.24(6)	1.64(7)	3.03(7)	4.09(7)	1.11(8)
C^+	12				3.25	9.67	11.91	23.89
CH^+	13				0.29	0.47	0.70	1.32
CH_2^+	14				0.22	0.23	0.26	0.50
CH_3^+	15				0.15			
C_2^+	24				0.65	3.69	4.38	10.25
C_2H^+	25				0.81	1.84	1.93	3.32
$C_2H_2^+$	26		0.20	3.52	3.58	3.32	3.33	4.22
$C_2H_3^+$	27		0.20	3.52	2.93	3.14	3.33	4.52
$C_2H_4^+$	28				0.33	0.28	0.18	0.31
C_3^+	36				6.22	11.44	10.30	12.07
C_3H^+	37			1.06	9.13	9.87	8.83	7.23
$C_3H_2^+$	38			1.06	3.11	2.34	2.31	1.61
$C_3H_3^+$	39	0.89	1.61	2.95	6.22	5.20	5.64	5.22
C_4^+	48				2.96	2.34	2.36	1.61
C_4H^+	49			0.72	5.93	4.35	4.34	2.82
$C_4H_2^+$	50		1.32	6.58	17.50	13.06	12.44	6.84
$C_4H_3^+$	51		4.13	12.19	14.23	10.04	10.09	4.89
$C_4H_4^+$	52	2.69	3.14	4.69	3.56	3.01	2.69	1.20
$C_5H_3^+$	63	0.22	0.40	0.94	0.99	0.43	0.70	
$C_6H_4^+$	76		2.98	2.95	1.01	0.87	0.95	0.40
$C_6H_5^+$	77		13.35	14.79	4.45	4.04	3.47	2.01
$C_6H_6^+$	78	89.84	66.75	41.36	11.57	9.53	9.15	5.22
	79	6.35	5.95	3.69	0.89	0.87	0.76	0.60

laser intensity is listed in table 1, expressed as percent of the total yield at that intensity. The same results are shown in bar graph form in fig. 2 and results for selected ions are plotted versus laser intensity in fig. 3.

The results are qualitatively similar to those of Reilly and Kompa [2]. We report a maximum of 22 different ions, compared to their 18, but the new species we detected were present only in low abundances, presumably below their sensitivity limit. The major and important difference between our results and theirs is in the intensity levels required to produce given fragmentation patterns. A visual comparison of their mass distributions with ours indicates similar patterns when our intensities are about one-tenth their stated values. As indicated above, we suspect that the actual laser intensities in their experiment were much lower than they calculated because the multimode excimer laser did not focus to as small a spot size as expected from simple diffraction theory. Our own experience, described above, shows that the discrepancy between the calculated and measured beam diameter can exceed a factor of 100.

In contrast, our results indicate somewhat less fragmentation at a given laser intensity than do those of Antonov et al. [3]. They report fragmentation of benzene beginning at 0.05 MW/cm^2, and their published mass spectrum at 2 MW/cm^2 shows similar levels of fragmentation as our results at 7 MW/cm^2. They report that $C_6H_6^+$ is the dominant ion at least up to 20 MW/cm^2, in reasonable agreement with our observation that it is dominant up to about 15 MW/cm^2. However, their fragmentation pattern is different in detail from those we observe at any laser intensity. In particular, their pattern for m/e = 76, 77, and 78 (corresponding to $C_6H_4^+$, $C_6H_5^+$, and $C_6H_6^+$), does not match our results for the same range of laser intensities. They made their measurements by reducing their laser beam size using a telescope, and then aperturing the reduced

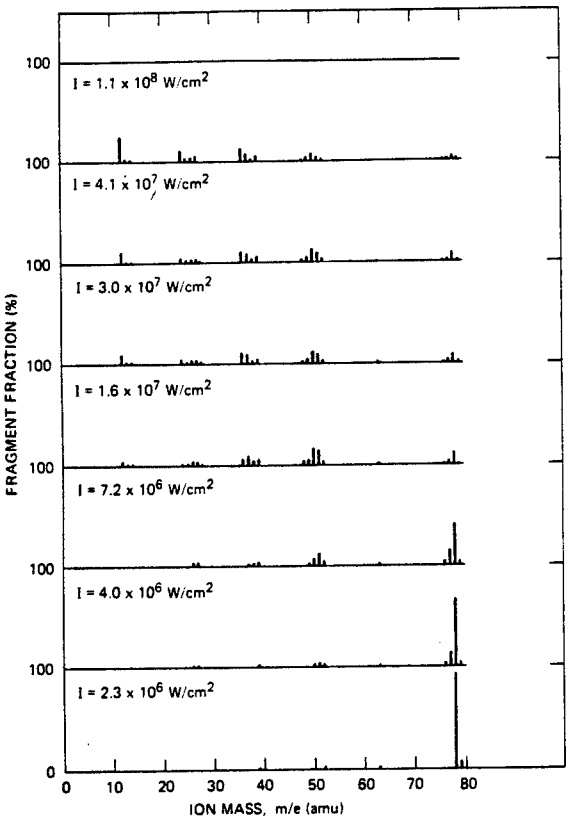

Fig. 2. Ion mass distribution resulting from photoionization of benzene at 248 nm as a function of laser power (14 ns fwhm of laser pulse).

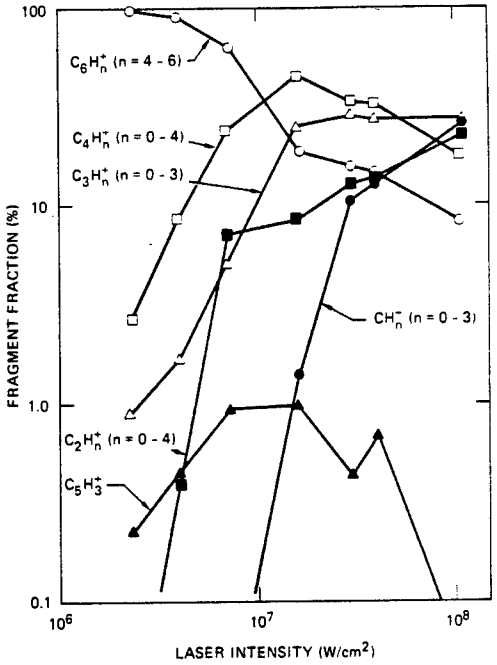

Fig. 3. Ion mass distribution for the most important fragment groups resulting from photoionization of benzene at 248 nm as a function of laser intensity.

beam. In order to achieve high laser intensities, they used up to 50% of the incident laser power. We suspect that the beam was non-uniform in intensity, so that there were "hot spots" in the reduced beam. Their fragmentation patterns would then result from the addition of larger areas of low intensity (primarily responsible for the parent ion signals) and localized areas of high intensity (which would contribute the majority of the fragment ion signals).

As suggested previously [2], benzene photoionization and fragmentation at 248 nm appears to occur by way of formation of the parent ion ($C_6H_6^+$), which subsequently absorbs more photons and decomposes stepwise, even as far as C^+ at the highest intensities. The yield of the parent ion decreases steadily over the entire intensity range. In addition, $C_6H_5^+$ and $C_6H_4^+$, which first appear at 4 MW/cm^2, decrease in constant proportion to $C_6H_6^+$ at higher intensities, as shown in fig. 2. The similarity of appearance intensities, together with their near equality of appearance energies, suggests that these two ions are both formed independently from the parent ion. Furthermore, their constant proportionality to the parent ion suggests that these two product ions undergo photodissociation at the same rate as the parent ion. As can be seen in figs. 2 and 3, the details of the photofragmentation spectrum of $C_6H_6^+$ are a complex function of the laser intensity. It appears that elimination of CH_n (n = 1–3) to yield $C_5H_3^+$ is not a favored process over the entire intensity range. Also, the elimination of C_2H_n (n = 0–4) seems to be favored over the extrusion of C_3H_n (n = 0–3) at intensities below 10^7 W/cm^2. The situation is complicated by the fact that the precursors (ionic or neutral) for the fragment ions are not presently known. However, the general trend can be noted, that the appearance energy for a fragment ion is inversely proportional to its carbon content (with the exception of $C_5H_3^+$).

We have added the contributions of ions of all

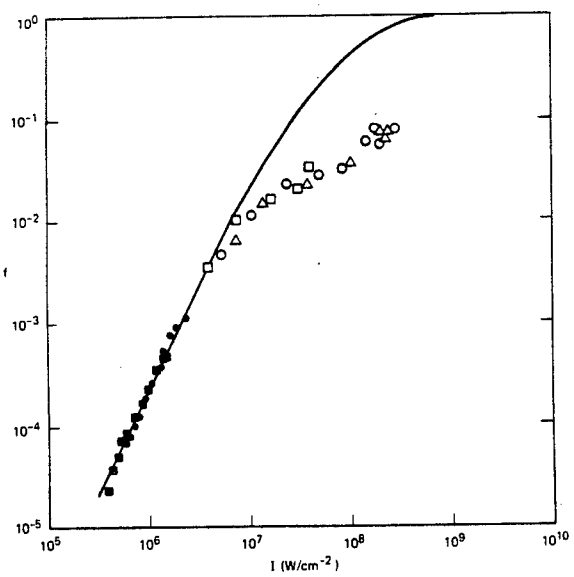

Fig. 4. Absolute ion yield (mass integrated) in resonant two-photon ionization of benzene at 248 nm as a function of laser power I (14 ns fwhm of laser pulse). ●, ■ ...unfocused beam, 80 Torr stagnation pressure, ○, △ ...focused, 0.8 Torr stagnation pressure, □ ...focused, 25 Torr stagnation pressure.

masses at each laser intensity to determine the dependence of total photoionization yield on laser power or intensity. The results are compared in fig. 4 with the predicted variation based on the molecular constants for benzene measured recently by Bischel et al. [7], using our laser pulse shape.

In their work, absolute ionization yields for the two-photon resonant excitation of benzene were measured at laser intensities low enough that no fragmentation occurred. The ion current was found to be strictly second order in laser intensity up to laser fluence of 8 mJ/cm^2, and the results were fitted to a four-level rate equation model of benzene. The assumption was made that photoionization only takes in benzene resulting in benzene molecular ion, $C_6H_6^+$, and therefore ionization of neutral fragments originating from the photodissociation of C_6H_6 or $C_6H_6^+$ would not contribute to the total observed ion current. This assumption also leads to the statement that all fragment ions must have their origin in $C_6H_6^+$, an assumption that may not hold in view of the low ionization potential of many open-shell hydrocarbon species. In fact, Bischel et al. were able to explain their data on the basis of the above assumption (no fragmentation under their experimental condition) and the following four-level model:

$$^1A_{1g} + h\nu \xrightarrow{\sigma_{10}} {}^1B_{2u}\,, \tag{1}$$

$$^1B_{2u} \xrightarrow{Q} {}^3B_{1u}\,, \tag{2}$$

$$^1B_{2u} \xrightarrow{\sigma_{21}} C_6H_6^+\,, \tag{3}$$

where $^1A_{1g}$ is the electronic ground state, $^1B_{2u}$ is the resonant intermediate state, $^3B_{1u}$ is the non-photoionizing lowest triplet state, and $C_6H_6^+$ is the ionic ground state of benzene; σ_{10} and σ_{21} are the corresponding absorption cross sections, and Q is the effective rate of deactivation of the resonant intermediate state with radiative (fluorescence) and non-radiative (intersystem crossing) components. With the aid of known values for σ_{10} of 3.7×10^{-19} cm^2 and Q of 2.2×10^7 s^{-1}, an ionization cross section of 4.4×10^{-18} cm^2 was found for σ_{21}, together with a small non-resonant two-photon cross section of $< 0.5 \times 10^{-27}$ cm^4/W [7].

The solid line in fig. 4 describes the absolute ionization yields using the above molecular parameters for benzene and our laser beam temporal profile. The low-intensity yields (black symbols in fig. 4) were then fitted to the calculated curve, because the absolute scale for the experimental points is arbitrary. The low-intensity data fit a second-order dependence on laser intensity rather well up to the point where fragmentation begins to become important (5% of total ion current at 2.5×10^6 W/cm^2 is distributed to lower-weight-fragment ions, see table 1). The high-intensity mass integrated ion yields (open symbols in fig. 4) were fitted such that the lowest two intensity data points coincided with the prediction from our rate equation model. The experimental results at intensities exceeding 7.5×10^6 W/cm^2 fall well below the prediction, which suggests either that an additional loss process "turns on" at higher laser power, or that space-charge effects reduce the collection efficiency for all ions at higher ion densities. However, the relative ionization yield for a variation of the benzene backing pressure of as much as a factor of 100 was found to be unchanged, which we take as an indication that space charge effects or recombination kinetics were not responsible for the depression of the MPI yield at higher laser power.

At this point our results lead us to postulate a neutral precursor state that can either undergo autoionization or absorb an additional photon to decay into neutral fragments. The depression of the MPI yield at higher laser intensities cannot be due to saturation effects because they have already been taken into account in the rate equation model. Furthermore, saturation effects are unimportant in the present case because $\sigma_{21} > 10\sigma_{10}$. This state is thought of as a superexcited state of benzene at an energy of twice the photon energy above ground state and is most likely a molecular Rydberg state of benzene. Using this neutral intermediate the resonant MPI scheme is given by

$$M + h\nu \rightarrow M^{*}, \quad (4)$$

$$M^{*} + h\nu \rightarrow M^{+} + e, \quad (5)$$

$$M^{*} + h\nu \rightarrow M^{**}, \quad (6)$$

$$M^{**} + h\nu \rightarrow A + B, \quad (7)$$

$$M^{**} \rightarrow M^{+} + e, \quad (8)$$

where M represents C_6H_6, M^{*} the one-photon resonant intermediate, and M^{**} the superexcited state of benzene.

4. Conclusions

We have reported careful quantitative measurements of the distribution of ions resulting from photoionization of benzene with a KrF laser at 248 nm. The fragmentation is extensive, as reported previously by Reilly and Kompa, but our measurements indicate that it occurs at about one-tenth the laser intensity that they reported. Our results are in reasonable agreement with those of Antonov, Letokhov and Shibanov, although their intensities for comparable fragmentation were even lower than ours. We have also reported absolute MPI yields at high laser powers which led us to postulate a neutral superexcited molecular state of benzene. The presence of this superexcited state is thought to be responsible for the depression of the absolute MPI yield with respect to the predicted yield for laser powers exceeding 7.5×10^{6} W/cm^{2}.

Acknowledgement

We are grateful to H. Helm for his assembling and testing the TOF mass spectrometer. This work was supported by the Defense Advanced Research Projects Agency through Office of Naval Research Contract N000 14-84-C-0718 and by the Army Research Office through Contract DAAG29-83-K-0113.

References

[1] S. Rockwood, J.P. Reilly, K. Hohla and K.L. Kompa, Opt. Commun. 28 (1979) 175.
[2] J.P. Reilly and K.L. Kompa, J. Chem. Phys. 73 (1980) 5468.
[3] V.S. Antonov, V.S. Letokhov and A.N. Shibanov, Appl. Phys. 22 (1980) 293.
[4] C.T. Rettner and J.H. Brophy, Chem. Phys. 56 (1981) 53.
[5] W.B. Martin and R.M. O'Malley, Intern. J. Mass Spectrom. Ion Phys. 59 (1984) 277.
[6] W.E. Martin, G.J. Caporaso, W.M. Fawley, D. Prosnitz and A.G. Cole, Phys. Rev. Letters 54 (1985) 685.
[7] W.K. Bischel, L.E. Jusinski, M.N. Spencer and D.J. Eckstrom, J. Opt. Soc. Am. B2 (1985) 877.
[8] N. Bjerre, R. Kachru and H. Helm, Phys. Rev. A31 (1985) 1206.